Thanh Truong Nguyen
Industrial Maintenance Training Center
Ho Chi Minh City University of Technology
Vietnam
Vietnam National University-Ho Chi Minh City
Vietnam

Thanh Hai Nguyen
Faculty of Mechanical Engineering
Ho Chi Minh City University of Technology
Vietnam
Vietnam National University-Ho Chi Minh City
Vietnam

Ha Quang Thinh Ngo
Faculty of Mechanical Engineering
Ho Chi Minh City University of Technology
Vietnam
Vietnam National University-Ho Chi Minh City
Vietnam

Investigation on the Mechanical Design of Robot Gripper for Intelligent Control Using the Low-cost Sensor

With the advent of Industry 4.0, there is a growing need for intelligent and automated robotic systems capable of performing complex tasks in the unknowen environments. This work focuses on the development of mechanical design for a robotic gripper and the implementation of intelligent manipulation for picking a target using a FANUC robot platform. The proposed method combines computational mechanics for the gripper, advanced motion control techniques, and a grasping control strategy to enable the robot arm to accurately and efficiently identify and pick a target object. To validate our approach, several experimental validations are conducted in various scenarios. It is well-acknowledged that the proposed work is feasible, effective, and applicable for a wide range of industrial applications.

Keywords: *Robotic gripper, mechanical design, intelligent control, pick-and-place, motion control.*

1. INTRODUCTION

In recent years, industrial robots have become an inte–gral part of modern manufacturing processes, enabling efficient production and precise automation [1, 2]. In particular, the industrial robot arm, known for its robus–tness and versatility, has gained significant prominence in various industrial sectors. One critical aspect of its functionality is the successful manipulation of objects, especially in tasks such as picking [3, 4] and placing targets [5-7].

Numerous studies have focused on the technical specifications of hand grippers [8, 9] as well as the integration of intelligent manipulation techniques [10, 11] for the precise picking of a target using an industrial robotic system. Indeed, robotic grippers play a pivotal role in securely grasping the target object, while intel–ligent manipulation techniques enhance the high per–formance of the robot arm to adapt to various charac–teristics of objects, including shapes, sizes, and orien–tations.

Moreover, the mechanical design of a robotic gripper is a critical factor that directly impacts the success of target picking [12-14]. This gripper must possess the versatility to handle various object types, spanning from delicate items to heavy components. It should offer secure and stable grasping actions while minimizing the risk of damage to the target object or the robot arm itself. Taking these requirements into account, an improved gripper design can markedly enhance the overall performance and efficiency of the picking process.

In addition, intelligent control schemes also play a vital role in enabling the robot platform to adapt to uncertainties and variations in target objects [15]. These techniques encompass advanced algorithms and sensors that enhance perception, planning, and control to ensure successful grasping and manipulation. By incorporating intelligent manipulation techniques, the robot manipulator can precisely identify the location of the target object, estimate its shape and orientation, and adjust its grasp accordingly [16].

2. LITERATURE REVIEW

The field of robotics has witnessed significant advan–cements in recent years, particularly in the realm of industrial automation. Various types of grippers [17] have been developed to meet diverse industrial requi–rements. Gripper kinematics and compliance directly influence their gripping ability and adaptability to different objects. Researchers have delved into the kine–matic modelling and analysis of grippers to optimize their grasping strategies. Compliance control methods [18], including compliant mechanisms and soft grippers, have been explored to enhance gripping force and adaptability to objects of various shapes and sizes. In related fields, some cutting-edge techniques are sum–marized in Table 1 over the past few years.

The integration of sensing and feedback systems within grippers has also garnered significant attention from scholars for precise object detection, force control, and feedback-based manipulation. Several studies [19, 20] have concentrated on the integration of sensors, including force/torque sensors, proximity sensors, and vision systems, to enhance the gripper's perception capabilities during the picking process.

In the other hand, both force and compliance control considerably guarantee the safe and accurate object manipulation. Researchers have explored advanced control algorithms, such as impedance control [33, 34], to regulate the applied forces during the grasping process, enabling robots to handle delicate or fragile objects without causing damage.

Received: September 2023, Accepted: November 2023
Correspondence to: Ha Quang Thinh Ngo, Faculty of Mechanical Engineering, Ho Chi Minh City University of Technology, 268 Ly Thuong Kiet Street, District 10, HCMC, Vietnam. E-mail: nhqthinh@hcmut.edu.vn
doi: 10.5937/fme2401012T

Table 1. List of the cutting-edge techniques in related fields.

Approach	Publication year	Author(s)	Problem statement	Proposed solution	Platform	Limitation(s)
Actuator for grasping task	2021	Hoang, T. T. et al [21]	Currently, the pro–duction method of soft grippers is mainly based on silicon mol–ds, which are simple but difficult to expand	Pneumatically operated multi-finger gripper, layered and variable stiffness	Rubber (self-made), pneumatic, pressure sensor force sensor	The clamping for–ce is quite small, which can lead to slipping or falling if there is vibration during the gripping process
	2018	Ngo, T. H. et al [22]	Most current grippers operate passively	Dual mechanism design allows active clamping and release action	N/A	Only suitable for small and micro objects
	2022	Vo, Q. N. et al [23]	Medical applications of soft structures lack fle–xibility and adaptability in hand rehabilitation	This study proposes a soft glove design to restore gripping function using a pneumatic mechanism	Elastic thread made of vinyl chloride, pneumatic valve	The design is quite simple, not suitable for the flexible movements of the fingers
	2022	Quach, B. M. et al [24]	Soft and flexible materials for biomimetic-inspired robotic gloves become key challenge	Electro-pneumatic glove consisting of micropro–cessor, pump, solenoid and valve for physiotherapy application was invented.	Microprocessor STM32F101C8T6, pneumatic pump, pressure sensor	The control of the angle of the finger is nonlinear
Robot hardware	2021	Anh-My, C. [25]	Small and medium loads are always one of the limitations of today's robots	In harsh conditions such as foundries, robots that have to work with high loads and high temperatures have been proposed	Hydraulic cylinder, hydraulic motor, 2-way 3-position valve, pump and oil tank	The rather slow response of the hydraulic mechanism can affect performance
	2022	Do, T. T. et al [26]	Today's needs require robots to cooperate with humans	Collaborative robot's open architecture and advanced features are presented	6 degrees of freed–om arm, NI Com–pactDAQ . controller	Research results have not been tested
Grasping task by traditional method	2021	Nguyen, T. H. et al [27]	In order to grasp ob–jects, the core problem in previous studies was the positioning of the object and the act of picking up the object.	The method includes col–lecting image data from Kinect camera, determi–ning image depth and calculating robot control	6 degrees of freedom arm, Kinect camera	The picking process has not been verified, the object recognition context is relatively simple
	2021	Hoang, H. H. et al [28]	Previous methods often have difficulty at the edges or edges of the object	By blending the 3D model to distinguish pixels into angular and masked areas, the proposed method de–monstrates superiority in harsh working conditions.	Kinect camera	Down-sampling technique can greatly affect the accuracy of object positioning
Grasping task by advanced method	2021	Le, T. T. et al [29]	High-level autonomous systems always enco–unter obstacles in the process of accurately picking up objects	A two-stage model inclu–ding object recognition by deep learning network and direction estimation by point feature set has been developed.	DENSO arm 6 degrees of freedom, EinScan-SED camera	Only suitable for static subjects and the grip mechanism is soft type
	2022	Hoang, D. C. et al [30]	Previous studies on autonomous robot systems mainly per–form tasks with known objects and require preprocessing steps	This work uses a deep learning network to control the collision avoidance trajectory when picking by a collection of a cloud of points in space.	Franka arm, ASUS Xtion PRO LIVE image sensor	Single action can be a hindrance in a chaotic environment
Several related applications	2019	Pham, H. D. et al [31]	Using the surgical robotic arm in practice always requires a lot of relevant knowledge and experience	Operation results are quite optimistic such as no com–plications in surgery, no open surgery, no cholan–gitis	8-mm and 5-mm robotic port, 5-mm laparoscopic port	High cost is a major barrier to wides–pread dissemination of this application
	2021	Lam, C. T. et al [32]	In everyday applications like refueling a car, the key point is the ability to open the fuel tank cap	A new design on the wor–king head that helps the robot to turn and pick up the gas cap has been pre–sented. Then, image pro–cessing techniques to reco–gnize the position and cont–rol the fuel nozzle. Algo–rithm to adjust the amount of fuel poured in accor–dance with the parameters of the fuel tank	Robotic arm 6 degrees of freedom, Kinect camera	The principles of more fluid movements such as delivery or throwing are not mentioned

DQN: Deep Q-learning, N/A: Not applied, CNN: Convolutional Neural Network

Grasp planning involves determining the optimal configuration of the gripper to achieve stable and suc–cessful grasping. Various algorithms and optimization techniques [35-39], including geometric and physics-based approaches, have been developed to generate feasible grasp configurations and improve the overall success rate of picking tasks.

3. THEORETICAL WORKS

3.1 Computational background

To manipulate the driving control, the architecture of manipulator platform must be analysed and studied. In our design, the five-DOF (Degree of Freedom) robot as Fig. 1 is deployed. These axes are labelled from the base to the end-effector.

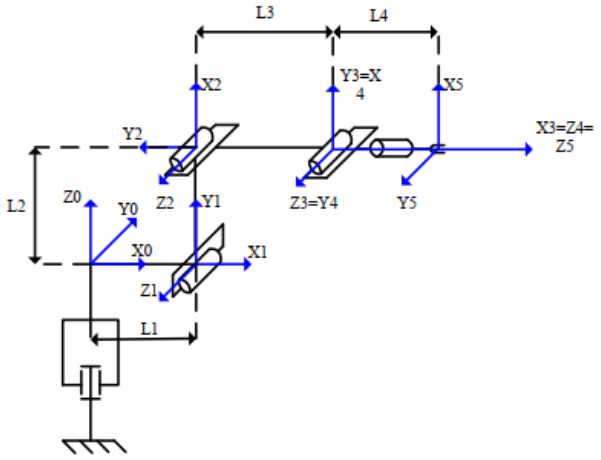

Figure 1. Notation and architecture of the proposed system

Henceforth, the description of the Denavit-Harten–berg (D-H) matrix should be established as Table 1.

Table 2. Description of parameters in D-H matrix

Link	Parameter			
	α_i (o)	a_i (mm)	d_i (mm)	θ_i (o)
1	90	L_1	0	θ_1
2	0	L_2	0	θ_2
3	0	L_3	0	θ_3
4	90	0	0	θ_4
5	0	0	L_4	θ_5

Consequently, the location of our end-effector is,

$$p_x = \cos\theta_1(L_1 + L_2\cos\theta_2 + L_3\cos(\theta_2+\theta_3) + L_4\sin(\theta_2+\theta_3+\theta_4)) \quad (1)$$

$$p_y = \sin\theta_1(L_1 + L_2\cos\theta_2 + L_3\cos(\theta_2+\theta_3) + L_4\sin(\theta_2+\theta_3+\theta_4)) \quad (2)$$

$$p_z = L_2\sin\theta_2 + L_3\sin(\theta_2+\theta_3) - L_4\cos(\theta_2+\theta_3+\theta_4) \quad (3)$$

The orientation of our end-effector is,

$$R_{XYZ}(\alpha,\beta,\gamma) = R_Z(\alpha)R_Y(\beta)R_Z(\gamma) \quad (4)$$

$$= \begin{bmatrix} \cos\alpha & -\sin\alpha & 0 \\ \sin\alpha & \cos\alpha & 0 \\ 0 & 0 & 1 \end{bmatrix} \begin{bmatrix} \cos\beta & 0 & -\sin\beta \\ 0 & 1 & 0 \\ -\sin\beta & 0 & \cos\beta \end{bmatrix} \times \begin{bmatrix} 1 & 0 & 0 \\ 0 & \cos\gamma & -\sin\gamma \\ 0 & \sin\beta & \cos\gamma \end{bmatrix}$$

$$= \begin{bmatrix} \cos\alpha\cos\beta & \cos\alpha\sin\beta\sin\gamma - \sin\alpha\cos\gamma & \sin\alpha\sin\gamma + \cos\alpha\sin\beta\cos\beta \\ \sin\alpha\cos\beta & \cos\alpha\cos\gamma + \sin\alpha\sin\beta\sin\gamma & \sin\alpha\sin\beta\cos\gamma - \cos\alpha\sin\gamma \\ -\sin\beta & \cos\beta\sin\gamma & \cos\beta\cos\gamma \end{bmatrix}$$

In addition,

$$R_{xyz}(\alpha,\beta,\gamma) = \begin{bmatrix} r_{11} & r_{12} & r_{13} \\ r_{21} & r_{22} & r_{23} \\ r_{31} & r_{32} & r_{33} \end{bmatrix} \quad (5)$$

Multiply by $R_z(\alpha)^{-1}$, we have

$$R_y(\beta)R_x(\gamma) = R_z(\alpha)^{-1}R_{xyz}(\alpha,\beta,\gamma)$$

$$\Leftrightarrow \begin{bmatrix} cos\beta & 0 & -sin\beta \\ 0 & 1 & 0 \\ sin\beta & 0 & cos\beta \end{bmatrix} \begin{bmatrix} 1 & 0 & 0 \\ 0 & cos\gamma & -sin\gamma \\ 0 & sin\beta & cos\gamma \end{bmatrix} = \begin{bmatrix} cos\alpha & -sin\alpha & 0 \\ sin\alpha & cos\alpha & 0 \\ 0 & 0 & 1 \end{bmatrix} \begin{bmatrix} r_{11} & r_{12} & r_{13} \\ r_{21} & r_{22} & r_{23} \\ r_{31} & r_{32} & r_{33} \end{bmatrix} \quad (6)$$

Comparing between two sides in equation (11),

$$-sin\alpha r_{11} + cos\alpha r_{21} = 0$$

$$\Rightarrow tan\alpha = \frac{r_{21}}{r_{11}} \Rightarrow \alpha = arctan\left(\frac{r_{21}}{r_{11}}\right) \text{ and } \alpha = \alpha + 180° \quad (7)$$

From row two column two and row two column three in equation (11),

$$\begin{cases} cos\beta = cos\alpha r_{11} + sin\alpha r_{21} \\ -sin\beta = r_{33} \end{cases}$$

$$\Rightarrow \beta = arctan\left(\frac{r_{33}}{cos\alpha r_{11} + sin\alpha r_{21}}\right) \quad (8)$$

From row one column one and row three column one in equation (11),

$$\begin{cases} cos\gamma = cos\alpha r_{12} + sin\alpha r_{22} \\ -sin\gamma = -sin\alpha r_{13} + cos\alpha r_{23} \end{cases}$$

$$\Rightarrow \gamma = arctan\left(\frac{sin\alpha r_{13} + cos\alpha r_{23}}{cos\alpha r_{12} + sin\alpha r_{22}}\right) \quad (9)$$

3.2 Inverse kinematics

In this section, both location and orientation of the end-effector are known.

$$ {}^{0}_{1}A^{-1}.{}^{0}_{5}A = {}^{1}_{5}A = {}^{1}_{2}A\,{}^{2}_{3}A\,{}^{3}_{4}A\,{}^{4}_{5}A \tag{10} $$

And,

$$ {}^{0}_{1}A^{-1} = \begin{bmatrix} cos\,\theta_1 & sin\,\theta_1 & 0 & -L_1 \\ 0 & 0 & 1 & 0 \\ sin\,\theta_1 & -cos\,\theta_1 & 0 & 0 \\ 0 & 0 & 0 & 1 \end{bmatrix} \tag{11} $$

$$ \begin{aligned} {}^{0}_{5}A &= \begin{bmatrix} r_{11} & r_{12} & r_{13} & p_x \\ r_{21} & r_{22} & r_{23} & p_y \\ r_{31} & r_{32} & r_{33} & p_z \\ 0 & 0 & 0 & 1 \end{bmatrix} \\ &= \begin{bmatrix} r_{11} & r_{12} & r_{13} & x \\ r_{21} & r_{22} & r_{23} & y \\ r_{31} & r_{32} & r_{33} & z \\ 0 & 0 & 0 & 1 \end{bmatrix} \end{aligned} \tag{12} $$

$$ {}^{1}_{5}A = \begin{bmatrix} c\,\theta_5 c(\theta_2+\theta_3+\theta_4) & -s\theta_5 c(\theta_2+\theta_3+\theta_4) \\ c\,\theta_5 s(\theta_2+\theta_3+\theta_4) & -s\theta_5 s(\theta_2+\theta_3+\theta_4) \\ s\,\theta_5 & -c\,\theta_5 \\ 0 & 0 \\ s(\theta_2+\theta_3+\theta_4) & -L_1 \\ -c(\theta_2+\theta_3+\theta_4) & 0 \\ 0 & 0 \\ 0 & 1 \end{bmatrix} \tag{13} $$

From row three column four of above equation, we have

$$ sin\,\theta_1 x - cos\,\theta_1 y = 0 \Rightarrow \theta_1 = arctan\left(\frac{y}{x}\right) \tag{14} $$

Because two following links are parallel, there is no result from the multiplication of reverse matrices. In the third link, we obtain

$$ {}^{3}_{4}A^{-1}\,{}^{2}_{3}A^{-1}\,{}^{1}_{2}A^{-1}\,{}^{0}_{1}A^{-1}\,{}^{0}_{5}A = {}^{4}_{5}A $$

$$ {}^{3}_{4}A^{-1}\,{}^{2}_{3}A^{-1}\,{}^{1}_{2}A^{-1} = \begin{bmatrix} cos(\theta_2+\theta_3+\theta_4) & sin(\theta_2+\theta_3+\theta_4) \\ 0 & 0 \\ sin(\theta_2+\theta_3+\theta_4) & -cos(\theta_2+\theta_3+\theta_4) \\ 0 & 0 \\ 0 & -L_2 cos(\theta_3+\theta_4)-L_3 cos\,\theta_4 \\ 1 & 0 \\ 0 & -L_2 sin(\theta_3+\theta_4)-L_3 sin\,\theta_4 \\ 0 & 1 \end{bmatrix} \tag{15} $$

where,

$$ {}^{0}_{1}A^{-1} = \begin{bmatrix} cos\,\theta_1 & sin\,\theta_1 & 0 & -L_1 \\ 0 & 0 & 1 & 0 \\ sin\,\theta_1 & -cos\,\theta_1 & 0 & 0 \\ 0 & 0 & 0 & 1 \end{bmatrix} \tag{16} $$

$$ \begin{aligned} {}^{0}_{5}A &= \begin{bmatrix} r_{11} & r_{12} & r_{13} & p_x \\ r_{21} & r_{22} & r_{23} & p_y \\ r_{31} & r_{32} & r_{33} & p_z \\ 0 & 0 & 0 & 1 \end{bmatrix} \\ &= \begin{bmatrix} r_{11} & r_{12} & r_{13} & x \\ r_{21} & r_{22} & r_{23} & y \\ r_{31} & r_{32} & r_{33} & z \\ 0 & 0 & 0 & 1 \end{bmatrix} \end{aligned} \tag{17} $$

$$ {}^{4}_{5}A = \begin{bmatrix} cos\,\theta_5 & -sin\,\theta_5 & 0 & 0 \\ sin\,\theta_5 & cos\,\theta_5 & 0 & 0 \\ 0 & 0 & 1 & L_4 \\ 0 & 0 & 0 & 1 \end{bmatrix} \tag{18} $$

Taking a balance between two sides at row one column three, we achieve

$$ \begin{aligned} &cos(\theta_2+\theta_3+\theta_4)cos\,\theta_1 r_{13} + \\ &cos(\theta_2+\theta_3+\theta_4)sin\,\theta_1 r_{23} + sin(\theta_2+\theta_3+\theta_4) r_{33} = 0 \\ &\Rightarrow \theta_2+\theta_3+\theta_4 = arctan\left(-\frac{cos\,\theta_1 r_{13} + sin\,\theta_1 r_{23}}{r_{33}}\right) \end{aligned} \tag{19} $$

From row one column four and row three column four, some equations could be reached

$$ \begin{cases} cos(\theta_2+\theta_3+\theta_4)(cos\,\theta_1 x + sin\,\theta_1 y) + sin(\theta_2+\theta_3+\theta_4) z \\ = L_2 cos(\theta_3+\theta_4) + L_3 cos\,\theta_4 + L_1 cos(\theta_2+\theta_3+\theta_4) \\ sin(\theta_2+\theta_3+\theta_4)(cos\,\theta_1 x + sin\,\theta_1 y) - cos(\theta_2+\theta_3+\theta_4) z \\ = L_2 sin(\theta_3+\theta_4) + L_3 sin\,\theta_4 + L_1 sin(\theta_2+\theta_3+\theta_4) - L_4 \end{cases} \tag{20} $$

Then,

$$ \begin{aligned} &[c(\theta_2+\theta_3+\theta_4(c\theta_1 x + s\theta_1 y) + s(\theta_2+\theta_3+\theta_4) z \\ &-L_1 c(\theta_2+\theta_3+\theta_4)]^2 + [s(\theta_2+\theta_3+\theta_4)(c\theta_1 x + s\theta_1 y) \\ &-c(\theta_2+\theta_3+\theta_4) z - L_1 s(\theta_2+\theta_3+\theta_4) - L_4]^2 \\ &= {L_2}^2 + {L_3}^2 + 2L_2 L_3 cos\,\theta_3 \\ &\Rightarrow cos\,\theta_3 = [c(\theta_2+\theta_3+\theta_4(c\theta_1 x + s\theta_1 y) + s(\theta_2+\theta_3+\theta_4) z \\ &-L_1 c(\theta_2+\theta_3+\theta_4)] + [s(\theta_2+\theta_3+\theta_4)(c\theta_1 x + s\theta_1 y) \\ &-c(\theta_2+\theta_3+\theta_4) z - L_1 s(\theta_2+\theta_3+\theta_4) - L_4]^2 \\ &-{L_2}^2 - {L_3}^2 / (2L_2 L_3) \\ &\Rightarrow cos\,\theta_3 = \frac{\left(c_{234}(c_1 x + s_1 y + s_{234} z - L_1 c_{234}\right)^2}{2L_2 L_3} \\ &\frac{+\left(s_{234}(c_1 x + s_1 y) - c_{234} z - L_1 c_{234} - {L_4}^2\right) - {L_2}^2 - {L_3}^2}{2L_2 L_3} \end{aligned} \tag{21} $$

$$ \Rightarrow \theta_3 = ar\,cos(cos\,\theta_3) \tag{22} $$

Next, the rotational angles of link 2, 4 and 5 are estimated by balancing between two sides at row one column four and row two column four, the following equations are:

$$\begin{cases} cos\,\theta_1 x + sin\,\theta_1 y - L_1 = L_2\,cos\,\theta_2 \\ +L_3\,cos(\theta_2+\theta_3) + L_4\,sin(\theta_2+\theta_3+\theta_4) \\ z = L_2\,sin\,\theta_2 + L_3\,sin(\theta_2+\theta_3) \\ -L_4\,cos(\theta_2+\theta_3+\theta_4) \end{cases} \quad (23)$$

$$\begin{cases} cos\,\theta_1 x + sin\,\theta_1 y - L_1 - L_4\,sin(\theta_2+\theta_3+\theta_4) \\ = (L_2 + L_3\,cos\,\theta_3)\,cos\,\theta_2 - L_3\,sin\,\theta_2\,sin\,\theta_3 \\ z + L_4\,cos(\theta_2+\theta_3+\theta_4) \\ = L_3\,sin\,\theta_2\,cos\,\theta_3 + (L_2 + L_3\,cos\,\theta_3)\,sin\,\theta_2 \end{cases}$$

We get

$$\Delta = \begin{vmatrix} L_3c_3 + L_2 & -L_3s_3 \\ L_3s_3 & L_2 + L_3c_3 \end{vmatrix} \quad (24)$$

$$\Delta_c = \begin{vmatrix} c_1x + s_1y - L_1 - L_4s_{234} & -L_3s_3 \\ z + L_4c_{234} & L_2 + L_3c_3 \end{vmatrix} \quad (25)$$

$$\Delta_s = \begin{vmatrix} L_3c_3 + L_2 & c_1x + s_1y - L_1 - L_4s_{234} \\ L_3s_3 & z + L_4c_{234} \end{vmatrix} \quad (26)$$

$$cos\,\theta_2 = \frac{\Delta_c}{\Delta} = \frac{L_3s_3(z + L_4c_{234})}{(L_3c_3 + L_2)(L_2 + L_3c_3) + L_3s_3L_3s_3} + \frac{(c_1x + s_1y - L_1 - L_4s_{234})(L_2 + L_3c_3)}{(L_3c_3 + L_2)(L_2 + L_3c_3) + L_3s_3L_3s_3} \quad (27)$$

$$sin\,\theta_2 = \frac{\Delta_s}{\Delta} = \frac{(L_3c_3 + L_2)(z + L_4c_{234})}{(L_3c_3 + L_2)(L_2 + L_3c_3) + L_3s_3L_3s_3} - \frac{(c_1x + s_1y - L_1 - L_4s_{234})L_3s_3}{(L_3c_3 + L_2)(L_2 + L_3c_3) + L_3s_3L_3s_3} \quad (28)$$

Then,

$$\Rightarrow \theta_2 = arctan\left(\frac{sin\,\theta_2}{cos\,\theta_2}\right) \quad (29)$$

θ_4 is computed as below

$$\theta_4 = \theta_{234} - \theta_2 - \theta_3$$

That we have

$$r_{32} = sin\,\theta_5\,sin(\theta_2+\theta_3+\theta_4)$$

$$\Rightarrow sin\,\theta_5 = \frac{r_{32}}{sin(\theta_2+\theta_3+\theta_4)} \quad (30)$$

$$\theta_5 = arcsin\left(\frac{r_{32}}{sin(\theta_2+\theta_3+\theta_4)}\right)$$

3.3 Theoretical computation of mechanical gripper

For the purpose of grasping the object so that the normal force acting on the object has a constant direction, the direction of the tool-end is always remained. With the requirement that the subject is to pick up an object with a size of 60x60mm, we must design the gripper so that the distance D between the two clamps must be greater than 60mm and the length of the right cheek L must be greater than 60mm. Theoretical diagram of our gripper is depicted as Fig. 2.

Hence, D = 80 mm and L = 60 mm.

It is required to select α so that when the clamp is folded, the arms do not touch each other, in addition, the thickness of the joints also affects the selection of α.

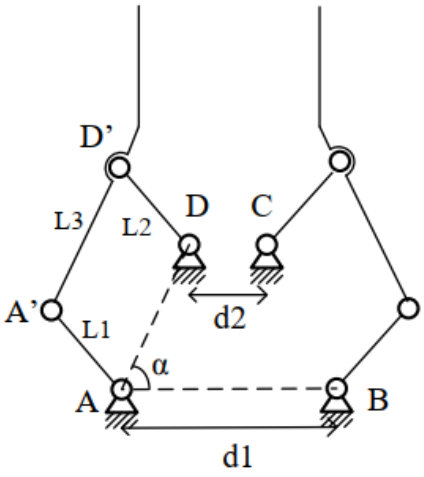

Figure 2. Theoretical diagram of mechanical gripper in our approach.

Owing to our knowledge, d_2 should be chosen so that the sizes of the intermediate joints do not overlap. Thus, d_2 = 20 mm, α = 110°.

Since two clamps are parallel, so $L_1 = L_2$ = 40 mm, $L_3 = AD = BC$ = 43 mm, d_1 = 50 mm, $d_3 = d_4$ = 43 mm.

In order not to damage the surface of the object when grasping as well as the force sensor, rubber is selected as the clamp. Henceforth, the friction coef–ficient is 0,6-0,7.

The acting force and its relation are analysed as Fig. 3 such gravitational force $\vec{P}$, pressing force from clamps $\vec{N}$, and friction force $\vec{F}_{ms}$. To hold an object, the following condition could be considered,

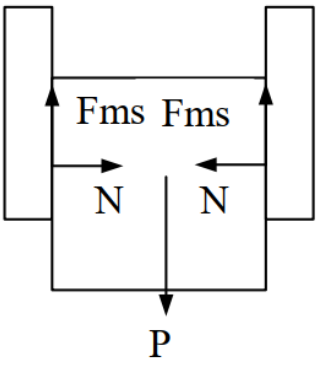

Figure 3. Analysis of the force exerted by the clamp on the object.

$$\begin{cases} \vec{P} = \vec{F}_{ms} \\ \vec{N} = \vec{F} \end{cases} \quad (31)$$

$$\Rightarrow N = F = \frac{MgS_F}{n\mu} = \frac{0,5 \times 9,81 \times 2}{2 \times 0,6} = 4,905(N)$$

Analytically, it is assumed that maximum force is reached when an object is hold at D = 60 mm, α = 60°. In Fig. 4a, according to Newton law, we have

$$\vec{F}_1 + \vec{F}_2 + \vec{N} + \vec{F}_{ms} = \vec{0} \tag{32}$$

In the O_{xy} coordinate, we obtain

$$\begin{cases} \sum F_x = F_1 \cos(60^o) - F_2 \cos(70,11^o) - \mathrm{N} = 0 \\ \sum F_y = F_1 \sin(60^o) + F_2 \cos(70,11^o) + F_{ms} = 0 \end{cases} \tag{33}$$
$$\Rightarrow \begin{cases} F_1 = 9,575N \\ F_2 = -9,956N \end{cases}$$

The sign '-'in above equation indicates that direction of force F_2 is reversed practically. Following as Fig. 4b, the condition to balance moment at point A is,

$$\sum M_A = F_2 \times L_2 \times \sin(49,88^o) - \mathrm{M} = 0$$
$$\Rightarrow M = 9,956 \times 0,04 \times \sin(49,88^o) = 0,305\,\mathrm{Nm} \tag{34}$$

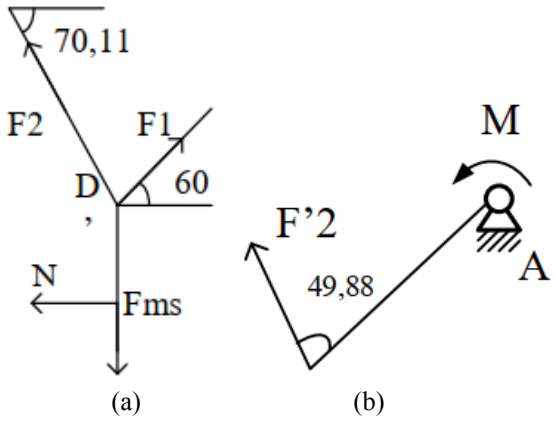

Figure 4. Mathematical analysis, (a) acting forces on AD' bar, and (b) balancing moment at point A.

As a result, using a pair of straight gears as transmission gears for the two clamps with axial distance $a_w = 50$ mm is our selection.

Modulus of gear should be computed as:

$$m = (0,01 \sim 0,02) \times a_w = 0,5 \sim 1 \tag{35}$$

Due to our evaluation, 3D design for the proposed gripper is illustrated as Fig. 5. This model uses an RC motor for drive. Two grippers and body of gripper machined by 3D printing, four crossbars straight and two gears made from mica. Since the maximum load of robot is only 3kg, hence light materials are utilized so as not to overload the robot.

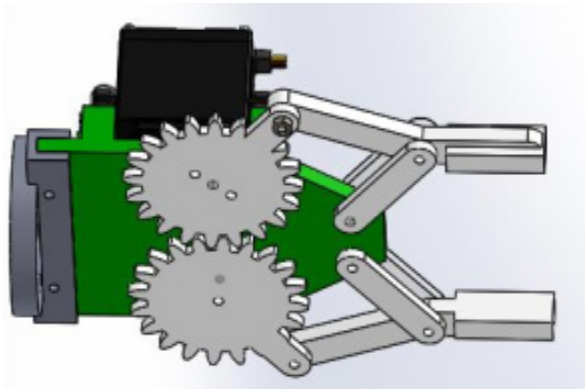

Figure 5. Mechanical design of our gripper in 3D.

When the RC motor drives the gears, the gear system has a gear ratio of 1. Thus, the two gears rotate at the same speed and in opposite directions. Because the mechanism used is a parallel mechanism, the two clamps always move parallel to each other and to ensure that the force acting on the object is always per–pendicular. Two gears drive the two sides of the jaws parallel in opposite directions to clamp the object. The mechanism is symmetrical so the initial angle of the two gears must be equal.

4. THE PROPOSED APPROACH

In order for a system to work, there are not only mechanical and control components, but also inter–mediate electrical devices, linking those components together, receiving signals and sending signals to the remaining components. This section is aimed at the computation and selection of sources and auxiliary devices, arrangement of equipment in the system.

4.1 Overall design of electrical diagram

This device that needs to be controlled in the system includes the RC motor on the gripper, force sensors, proximity sensors. In addition, there are separated sour–ces, one for control and one for driving. Main CPU collects data from sensing devices and orders the motion command to RC motor. Data transmission is completed via wireless communication between host computer and CPU. In the visual panel on host computer, an operator could monitor and manage whole system. The electrical connection of our system is demonstrated as Fig. 6.

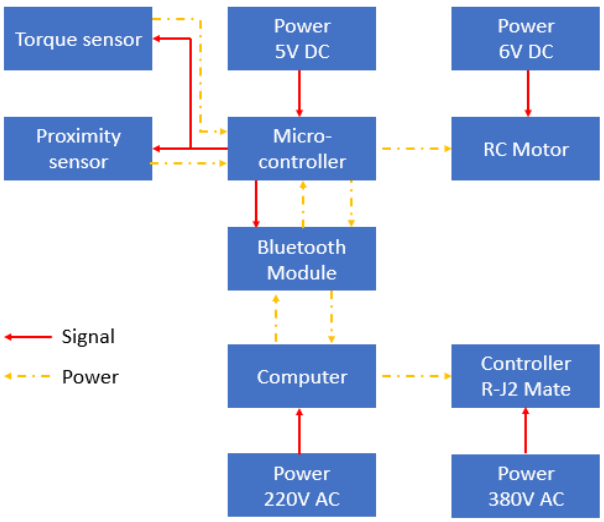

Figure 6. Block diagram of electrical design.

4.2 Sensor calibration

The main purpose of this force sensor calibrator is to use a system as follows for signal acquisition and signal processing. To calibrate the sensor accurately, it is necessary to solve the following problems: select the appropriate system to survey and determine the characteristics of sensor. To solve the problem of sensor data system, the data would be amplified operating according to the selected voltage as the system.

Secondly, to determine the characteristic, it is essential to sample many times to find the most suitable value for the resistance of the system and to keep the output voltage of the system within the range required by the microcontroller. In addition to obtain the sensor response graph using a range of masses as shown in Fig. 7, it could obtain the sensor output data.

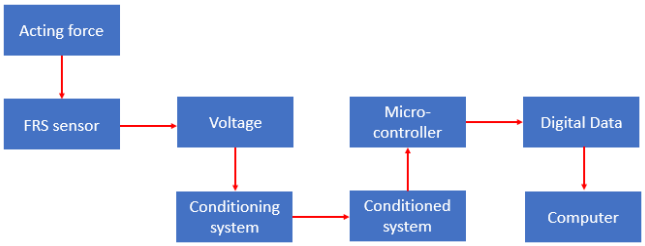

Figure 7. Flowchart of sensor calibration.

Signal conditioner, using an amplifier that acts as a voltage divider circuit, the output voltage is calculated as below

$$V_{out} = V_{in} \frac{R_m}{R_m + R_S} \tag{36}$$

where R_m is the fixed resistance value when we set it, R_S is the variable resistance value from the sensor. The above equation shows the relationship between the sensor resistance and the output voltage (depending on the applied force). On the other hand, the dependency graph between R_S and F follows the following formula,

$$R_S = a \times F^b \tag{37}$$

where a and b are the estimated coefficients from manufacturer

To construct the response, a series of data points are taken. From these values, we get the relationship between force and resistance in the form as below,

$$\ln(R_S) = b \ln(F) + \ln(a) \tag{38}$$

where R_S, F have unit as $k\Omega$ and g.

From the values obtained from the sensor when the load is changed, we get the following table of data as Table 2: Based on these parameters, the relationship between output signal and acting force is shown as Fig. 8. To discover the interpolated line between points, Least Square method is utilized to strengthen. Fig. 9 depicts the relationship between two parameters such ln(R_S) and ln(F).

Table 2. Experimental tests of sensor calibration.

No	Parameter			
	Input	ADC	Input	ADC
1	0	0	428	754.6
2	36	0	484	765.8
3	92	366.6	540	781.2
4	148	518,8	596	793.6
5	204	612,8	651	803.8
6	260	659,8	706	813.4
7	316	697,2	761	820.2

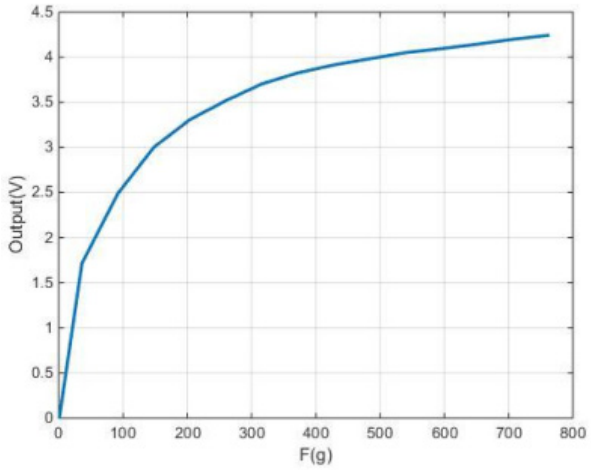

Figure 8. Diagram of relationship between output signal and acting force.

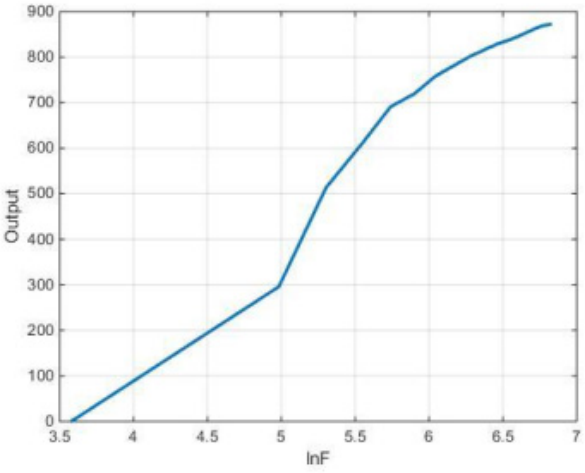

Figure 9. Diagram of relationship between ln(R_S) and ln(F)

4.3 Controller design

During the picking process, the most important thing is to keep enough force so that the object does not slip and deform (for objects with easily deformed surfaces). When the object reaches the grasping position, the proximity sensor would receive a value to activate the controller on the gripper. Control scheme on the end-effector would be the force controller. It is used to adjust the clamping force value so that the clamping object is not deformed or damaged. Therefore, the overall diagram of control scheme in the proposed approach is produced as Fig. 10.

When the motor on the gripper rotates faster, then when clamping on the object, the force would be greater. Subsequently, our controller needs to change the speed of the motor when the pressure from the both clamps acting on the object changes. Also, the force sensor would be in each clamp. The signal from the sensor would be fed back to the controller. For this control purpose, a characteristic of force sensing is when the gripper holds the object at a given motor speed.

To integrate the grasping strategy into the robot platform, the target location of an object should be provided. In this research, we do not focus on the vision-based technique. Thus, it is assumed that robotic system can identify target object and easily obtain its

coordinate. Then, the movements and poses of each link could be known via the inverse kinematic computations. This data is transferred to the motion planner which handle the multiple axes control. During the tracking trajectory, using forward kinematic to generate a set of reference points is necessary. After reaching to the target position, the proposed controller of gripper is activated so that it drives both fingers smoothly and securely.

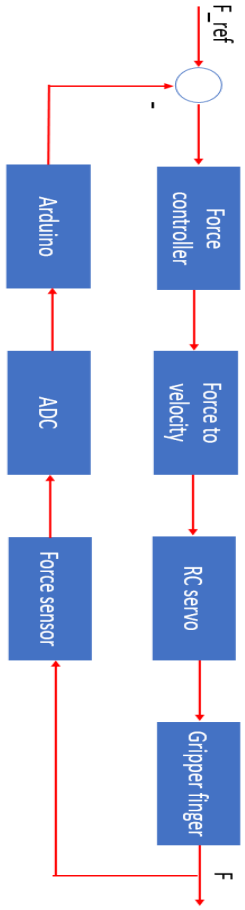

Figure 10. Diagram of the proposed controller.

A. Case 1: No load

In general, our gripper has symmetric shape and balancing design as Fig. 11a. Thus, without loss of generality, partial diagram of mechanical gripper is considered as Fig. 11b. It is assumed that the mass of joint is negligible. When grasping, two clamps which interact with an object, suffer acting force $\vec{F}$ including normal reaction force $\vec{N}$ and friction force $\vec{F}_{ms}$.

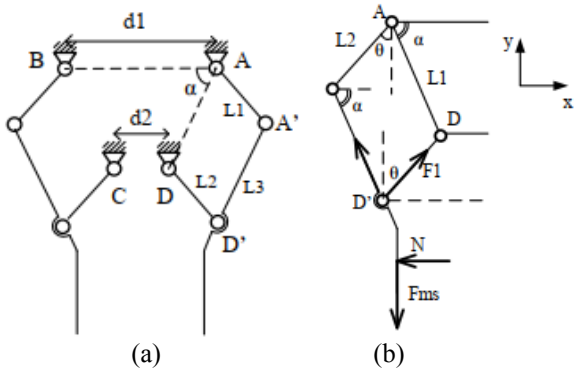

Figure 11. Theoretical design of mechanical gripper without load, (a) full diagram and (b) partial diagram.

In the A'D' bar, we have

$$\sum \vec{F} = \vec{N} + \vec{F}_{ms} + \vec{F}_1 + \vec{F}_2 = \vec{0} \tag{39}$$

In the O_x and O_y

$$\begin{cases} -N + F_1 \sin\theta - F_2 \cos\alpha = 0 \\ -F_{ms} + F_1 \cos\theta + F_2 \sin\alpha = 0 \end{cases}$$

$$\Leftrightarrow \begin{cases} F_1 = N \dfrac{\mu \sin\alpha + \cos\alpha}{\cos(\alpha - \theta)} \\ F_2 = N \dfrac{\mu \sin\theta - \cos\theta}{\cos(\alpha - \theta)} \end{cases} \tag{40}$$

As Fig. 12, moment at point A is,

$$\begin{aligned} M &= F_{2x} L_2 \cos\theta + F_{2y} L_2 \sin\theta \\ &= F_2 L_2 (\cos\alpha \cos\theta + \sin\alpha \sin\theta) \end{aligned} \tag{41}$$

Or,

$$\begin{aligned} M &= F_2 L_2 \cos(\alpha - \theta) \\ &= \mathrm{N} \frac{\mu \sin\theta - \cos\theta}{\cos(\alpha - \theta)} L_2 \cos(\alpha - \theta) = \mathrm{N} L_2 (\mu \sin\theta - \cos\theta) \end{aligned} \tag{42}$$

In the scope of kinetics, the movement of gripper is analysed as

$$v = \omega L_2 = \dot{\theta} L_2 \tag{43}$$

$$v_x = v \cos\theta = \dot{\theta} L_2 \cos\theta \tag{44}$$

Reversely, the dynamic equation of driving motor is

$$J\ddot{\theta} + b\dot{\theta} = \tau \tag{45}$$

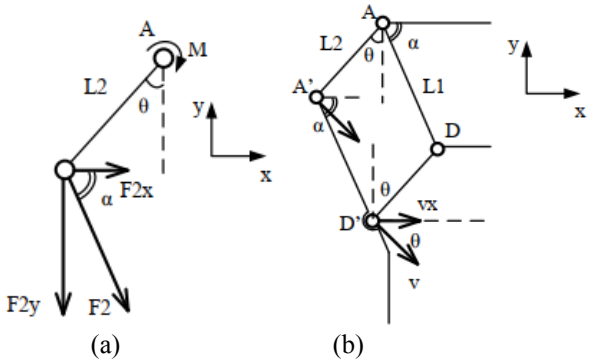

Figure 12. Analytical forces at point A (a) and analytical kinetics (b).

From the relationship between moment of motor, N and θ, we have

$$J\ddot{\theta} + b\dot{\theta} = NL_2(\mu \sin\theta - \cos\theta) \tag{46}$$

We get $f(\theta) = L_2(\mu \sin\theta - \cos\theta)$, then

$$J\ddot{\theta} + b\dot{\theta} = Nf(\theta) \tag{47}$$

$$J\dot{\omega} + b\omega = Nf(\theta) \tag{48}$$

Discretizing above equation, we obtain

$$J\frac{\omega_i - \omega_{i-1}}{dt} + b\omega_i = Nf(\theta_i) \tag{49}$$

B. Case 2: With load

In the case that gripper holds an object, this system has theoretical diagram as Fig. 13. Because the mechanism is symmetrical, it is considered that the force exerted by the clamp on the object and the displacement x of the two clamps are the same. The mass in two sides is $m_1 + m_2 = m$, where m is the mass of the object.

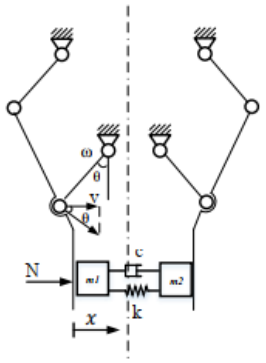

Figure 13. Theoretical design of mechanical gripper with load.

In this situation, the dynamical equation is

$$m_1\ddot{x} + 2c\dot{x} + 2kx = N \tag{50}$$

where, m_1 is the mass of partial clamp, and $m_1 = m_2 = m/2$because of symmetrical shape, c is the damping coefficient, k is the stiffness of spring, N is the magnetic reaction force acting on the object by the clamp.

Hence,

$$v = \dot{x} = \omega L_2 \cos\theta \tag{51}$$

where, v is the linear speed of the object m_1, ω is the rotational speed of the motor, θ is the rotational angle of the motor, L_2 is the stitch length of the gripper.

From above analysis, the PID (Proportional-Integral-Derivative) control scheme is

$$\frac{N(s)}{\Omega(s)} = K_P\left[1 + \frac{1}{T_i s} + T_d s\right] \tag{52}$$

From the view of backward difference method [33, 34], we have

$$u_F(t) = e_F(t)K_P\left[1 + \frac{T_S}{T_i(1-z^{-1})} + \frac{T_d(1-z^{-1})}{T_S}\right] \tag{53}$$

Simplify above equation,

$$\begin{aligned} u_F(t) &= u_F(t-1) + K_P\left[e_F(t) - e_F(t-1)\right] \\ &+ \frac{K_P T_S}{T_i} e_F(t) + \frac{K_P T_d}{T_S}\left[e_F(t) - 2e_F(t-1) + e_F(t-2)\right] \end{aligned} \tag{54}$$

where, $e_F = N_{ref} - N$ and $u_F = \omega$.

5. RESULTS OF STUDY

To validate the effectiveness and feasibility of our de–sign, the real-world system is built as Fig. 14. The robot platform comprises five-DOF (Degree-of-Freedom) LR Mate 100i FANUC, electrical cabinet, tech pendant and base table. This system works with three phase 380V power and voltage regulator source. To manipulate the robot drive, host computer which uses Windows 10 OS, is connected via USB cable. Most of programming works is completed by Visual Studio C/C++ language.

Figure 14. Experimental setup of the proposed system.

In this section, both simulation and experiment are carried out to verify the properness of theoretical com–putation and potential application. In each validation, test condition is like maintain the properties of our approach.

5.1 Numerical simulation

Owing to the controller design, several control gains are chosen as $K_P = 0.3$; $K_I = 0.65$, and $K_P = 0.001$. Sampling time is 0.1s, the initial angle of clamp is 20^o, and reference value of force is 0.001N. There are two competitive cases, case 1 for PI scheme and case 2 for our scheme. With our best knowledge, some differences between the initial grasping conditions are denoted. Hereafter, the condition $\omega_0 = 0$ means that an object is initially placed in the working area of gripper. There is no rotation or movement of an object when two clamps are activated.

The simulation results of two cases are demonstrated in Fig. 15, Fig. 16, Fig. 17 and Fig. 18. In these tests, the acting force and motor speed are represented as main parameters to compete. For easier comparison, Fig. 19 and Fig. 20 exemplify the system performance. It is clearly seen that there is no alteration between two cases in the same test condition.

In the second test, three cases are considered such case 1 for PD scheme, case 2 for PI scheme and case 3 for our scheme. Remember that $\omega_0 = 0.02$ (rad/s) means our gripper needs to react to an object.

Accordingly, the simulation results of acting force and motor speed for three cases are shown as Fig. 21, Fig. 22, Fig. 23, Fig. 24, Fig. 25 and Fig. 26. Additionally, the competitive results among three cases are described as Fig. 27 and Fig. 28. By visual observation, it could be resolved that our system reaches to stable state with short rising time and less peak although it suffers a little bit overshoot.

In detail, some values from our measurements in the simulation tests are listed as Table 3. From those results, PD scheme is not appropriate since the desired force is not met. For PI and PID controllers, the results are similar in terms of overshoot and settling time. Because

the application of this study does not require fast response time, PI or PID scheme is properly chosen. The initial velocity when the clamp hits the object has an effect on the response of the system because when the clamp with high velocity hits the object, a large impact force is generated on the clamp (assuming the same duration of action).

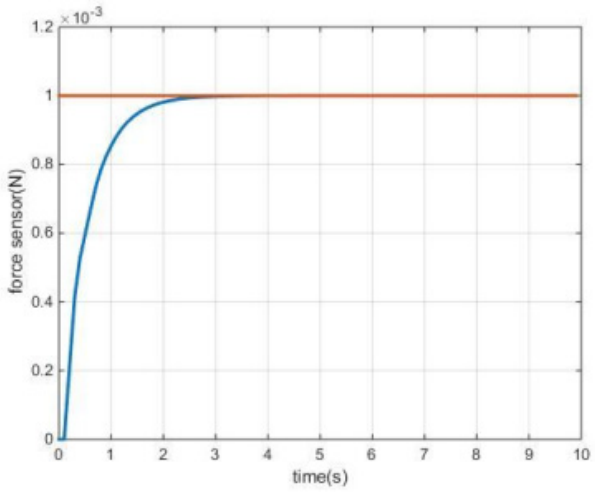

Figure 15. Simulation result for the response of acting force in case 1 with $\omega_0 = 0$.

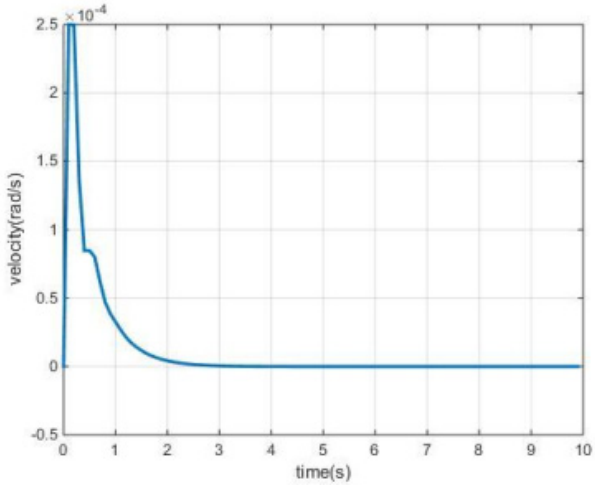

Figure 16. Simulation result for the response of motor speed in case 1 with $\omega_0 = 0$.

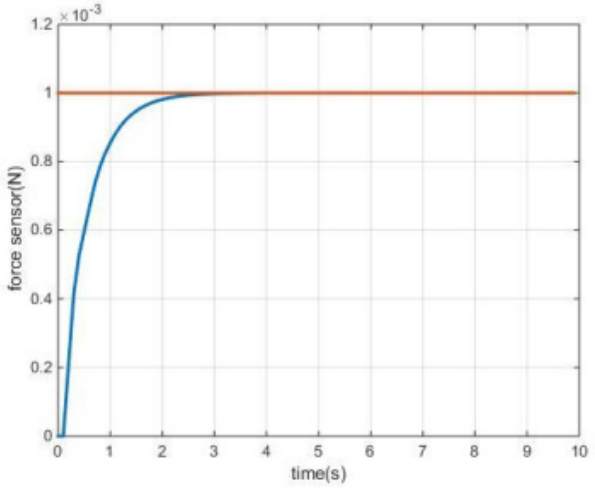

Figure 17. Simulation result for the response of acting force in case 2 with $\omega_0 = 0$.

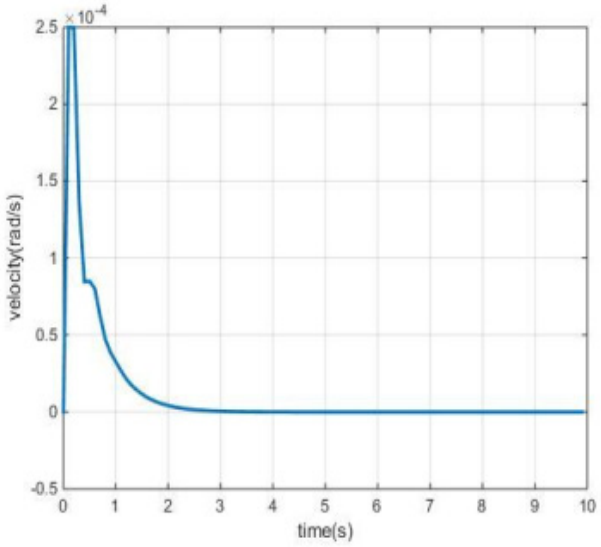

Figure 18. Simulation result for the response of motor speed in case 2 with $\omega_0 = 0$.

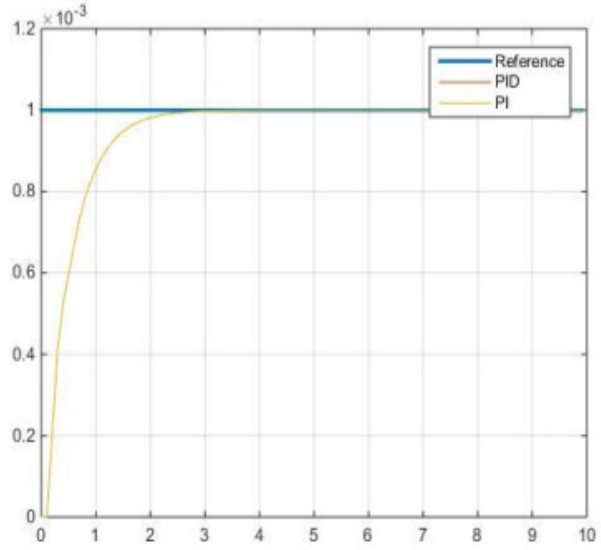

Figure 19. Comparative result in simulation for the response of acting force between two cases with $\omega_0 = 0$.

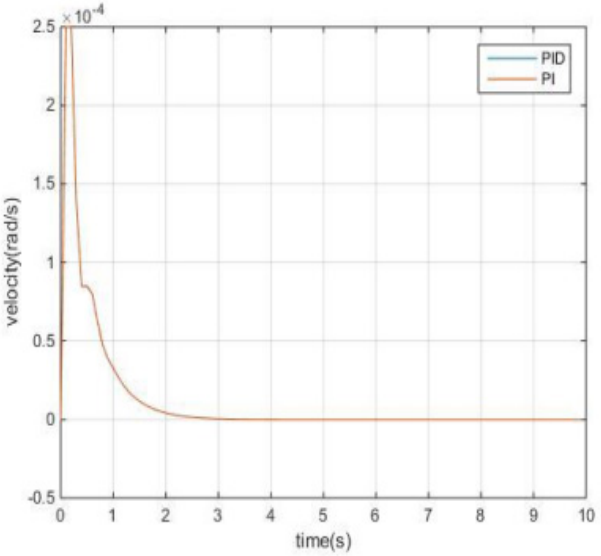

Figure 20. Comparative result in simulation for the response of motor speed between two cases with $\omega_0 = 0$.

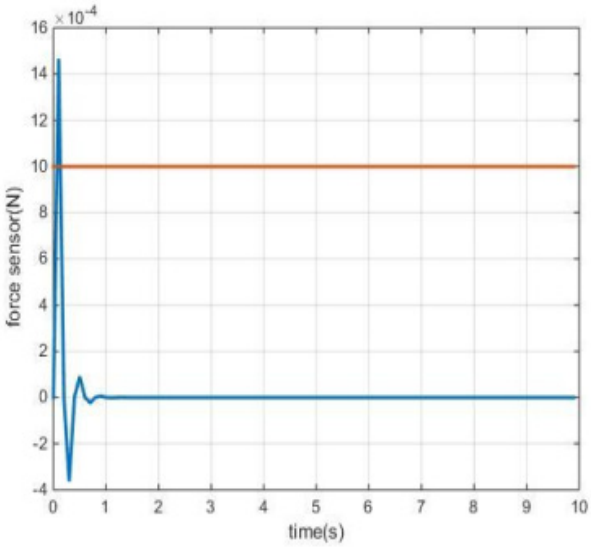

Figure 21. Simulation result for the response of acting force in case 1 with ω_0 = 0.02.

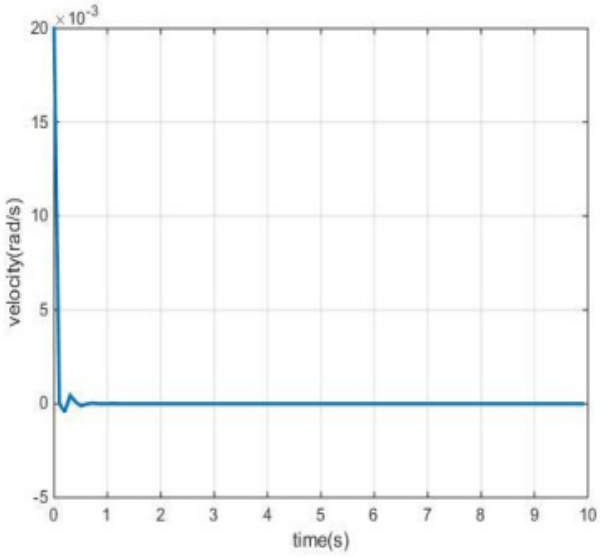

Figure 22. Simulation result for the response of motor speed in case 1 with ω_0 = 0.02

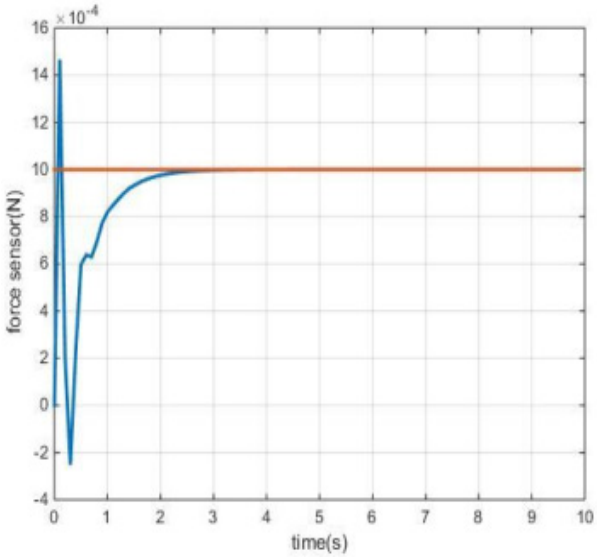

Figure 23. Simulation result for the response of acting force in case 2 with ω_0 = 0.02

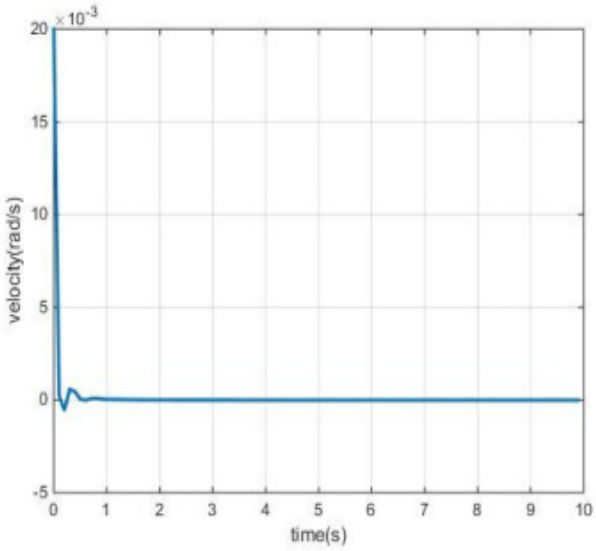

Figure 24. Simulation result for the response of motor speed in case 2 with ω_0 = 0.02

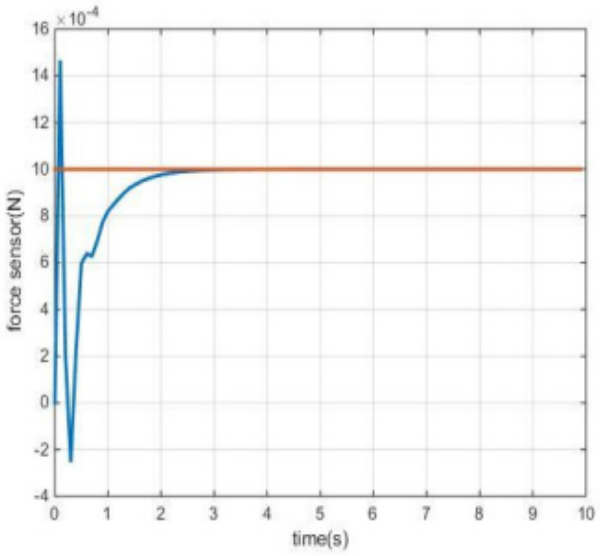

Figure 25. Simulation result for the response of acting force in case 3 with ω_0 = 0.02

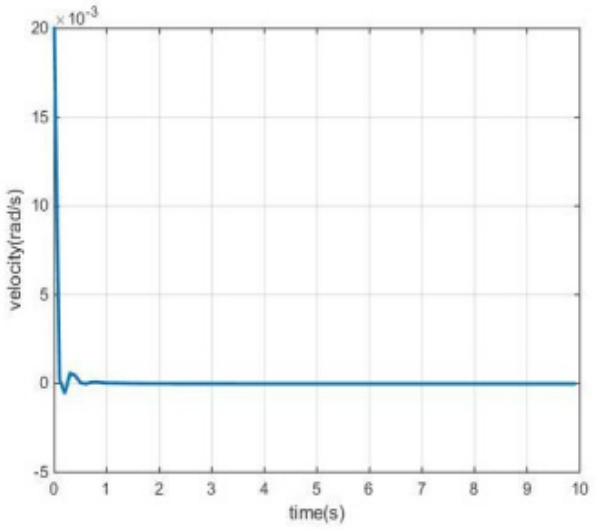

Figure 26. Simulation result for the response of motor speed in case 3 with ω_0 = 0.02.

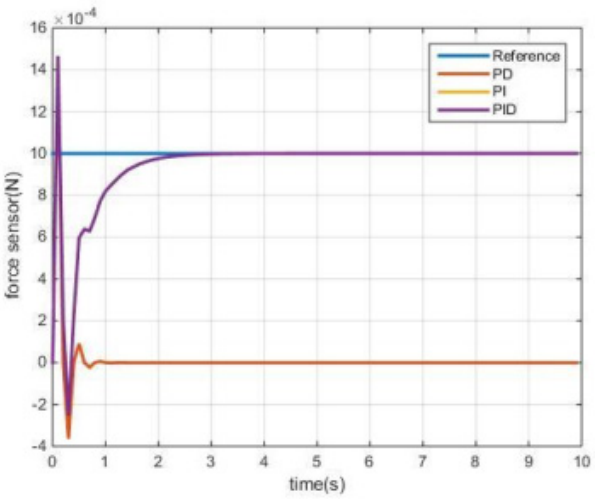

Figure 27. Comparative result in simulation for the res–ponse of acting force between three cases with ω_0 = 0.02.

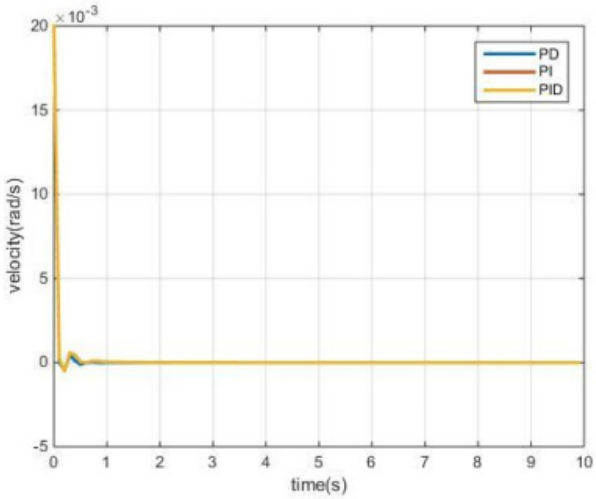

Figure 28. Comparative result in simulation for the res–ponse of motor speed between three cases with ω_0 = 0.02.

5.2 Experimental validation

With the coefficients of *PID* scheme, they are calculated from simulation and adjusted through experiment. Tuning values are s $K_P = 0.3$; $K_I = 0.65$, and $K_P = 0.001$, sampling time is 0.1s. To examine the controller, different force thresholds are set such $F_1 = 1.96N$ or 196g corresponds to the analogue value of the sensor is 500, $F_2 = 2.83N$ or 283g corresponds to the analogue value of the sensor is 600. In the experimental verification, robot picks up the object in two directions: the gripper is placed vertically and the gripper is placed horizontally.

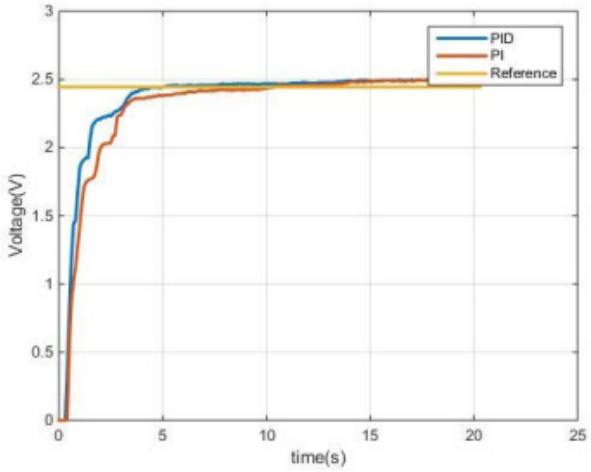

Figure 29. Experimental result in analogue value for vertically grasping direction with threshold F_1.

The practical verification includes several steps as following:

+ Insert the position of the points so that the robot follows a fixed trajectory

+ When the robot reaches the position to pick up the object, the infrared sensor identifies the object, the gripper picks up the object and returns the analogue value on the computer screen

+ After that, the robot continues to move to the end position

+ With a fixed trajectory, it could determine the time of movement from the initial position to the final position. Because our operator could not communicate with the robot, teach-pendant is only used to control. So, to let the gripper release the object, an operator uses the timer to interrupt.

The validated sample is a foam box for testing with force applied to the clamps. For the test sample which is weighted as 5g, the desired clamping force is sufficient to hold the object. In the vertically grasping direction, Fig. 29 and Fig. 30 represent the values of measurement from sensor and force for threshold F_1 respectively, while those values are portrayed as Fig. 31 and Fig. 32 for threshold F_2 correspondingly. Similarly, some results in values of analogy and force are measured in the horizontally grasping direction for two thresholds as Fig. 33, Fig. 34, Fig. 35 and Fig. 36 individually.

Table 3. List of simulation results for various test cases with ω_0 = 0 and ω_0 = 0.02.

Parameter	Measuring value				
	$\omega_0 = 0$		$\omega_0 = 0.2$		
	PI	Our scheme	PI	PD	Our scheme
Rising time	1,0351	1,035	0,0546	0	0,0546
Settling time	1,9726	1,9723	1,9885	0,5651	1,9879
Overshoot	2,1477.10-4	2,1493.10-4	46,6090	1,2430.1018	46,6090
Peak	0,0010	0,0010	0,0015	0,0015	0,0015
Peak time	7,2000	7,2000	0,1000	0,0015	0,1000

PI: Proportional-Integral, PD: Proportional-Derivative

Table 4. List of experimental results for various test cases with threshold F_1 = 1,93N and threshold F_2 = 2,83N.

Parameter	F_1 = 1,93N				F_2 = 2,83N			
	Horizontal		Vertical		Horizontal		Vertical	
	PI	Our scheme	PI	Our scheme	PI	Our scheme	PI	Our scheme
Rising time	4.8203	1.9845	2.5931	2.2303	3.910	2.3104	2.3543	2.5152
Settling time	12.28	4.2980	10.4760	5.1390	7.4660	4.1440	4.4880	5.6880
Settling Min	460	465	466	460	557	550	551	548
Settling Max	511	502	513	511	617	607	613	606
Overshoot	0.1961	0.1996	0.1953	0	0	0.1650	0.1634	0
Peak	511	502	513	511	617	607	613	606
Peak time	19.7	18.20	19	16,40	20.20	20	17.90	19.5

PI: Proportional-Integral

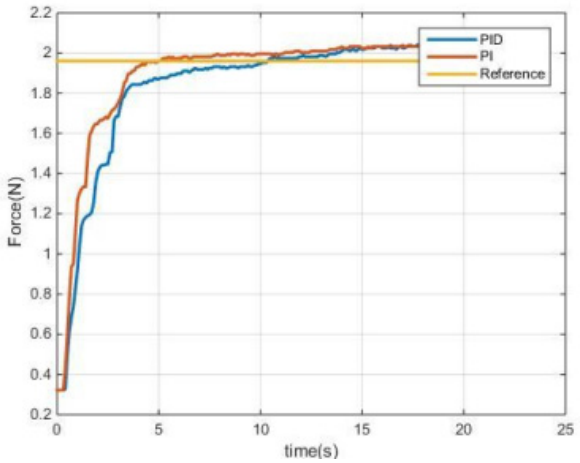

Figure 30. Experimental result in force value for vertically grasping direction with threshold F_1.

For more details, a list of measurements in our vali–dations is recorded as Table 4. It is noted that there are additional parameters such that minimum and maximum value of settling time is attracted because our experi–ments are repeated in several times to ensure the correctness. From our achievements, it is clearly seen that the response time of this system using our control scheme is better whilst the overshoot in the case of vertically grasping direction is more superior.

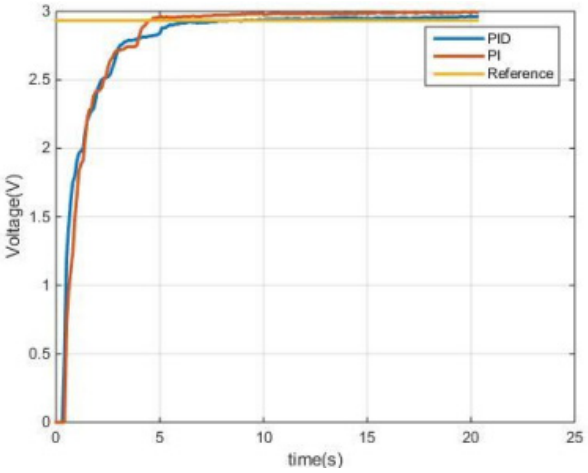

Figure 31. Experimental result in analogue value for vertically grasping direction with threshold F_2.

In this method, our contributions are to (a) establish the relative constraints between robot configuration and its end-effector, (b) propose the force-enabled controller for grasping action of robotic gripper, and (c) evaluate the effectiveness and feasibility of our approach in different test scenarios. In the same domain, most of previous studies focussed on the vision-based strategies which could estimate the direction, pose or location of an object in 3D workspace. The proposed technique co–uld assess the stiffness of surface of one object, then it is able to sensitively resolve how to capture. Especially, if an object is soft and fragile, this controller could handle the grasping actions safely and comfortably.

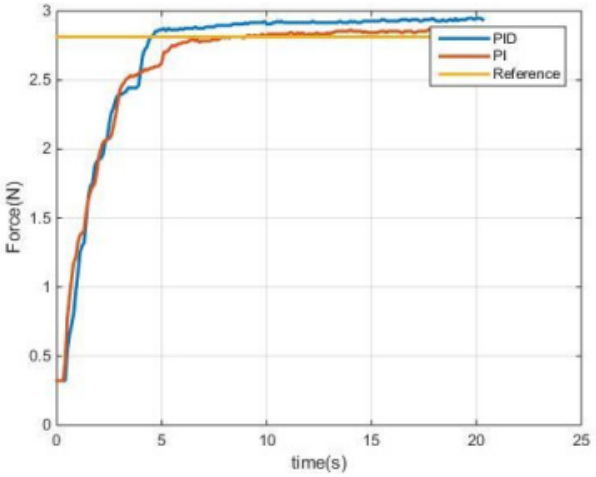

Figure 32. Experimental result in force value for vertically grasping direction with threshold F_2.

Reversely, although the proposed approach is fea–sible and effective, some requirements must be acknow–ledged when using this technique. Since the force control is very sensitive, the high quality of sensing device should be invested. Furthermore. the control gains must be tuned due to the experiences of an operator. It requires the expert-based knowledge as well as time consuming in order to drive this system without any accident.

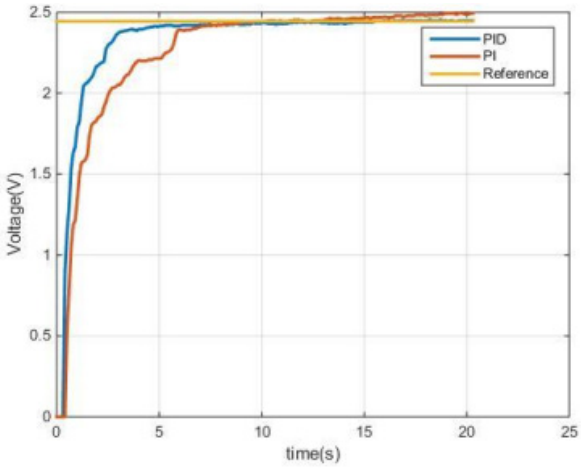

Figure 33. Experimental result in analogue value for horizontally grasping direction with threshold F_1.

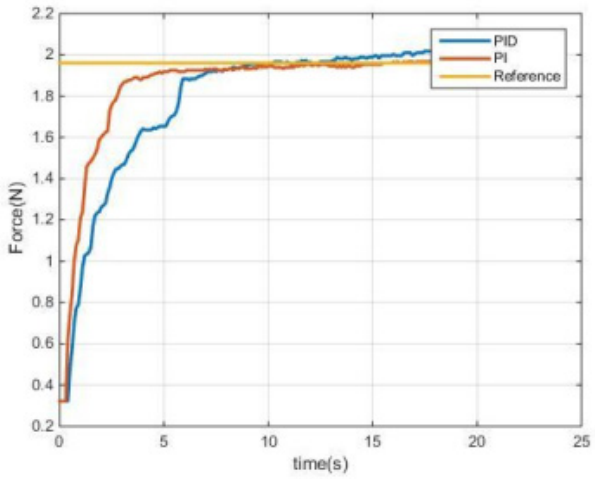

Figure 34. Experimental result in force value for horizontally grasping direction with threshold F_1.

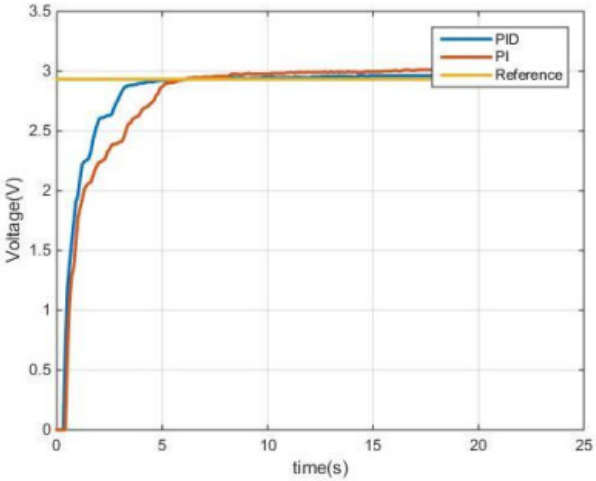

Figure 35. Experimental result in analogue value for horizontally grasping direction with threshold F_2.

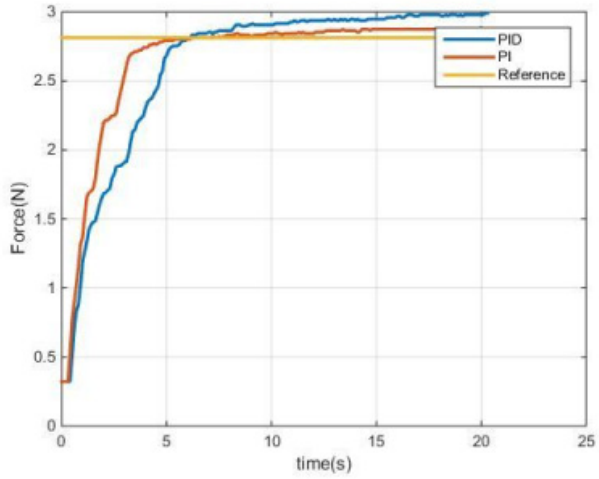

Figure 36. Experimental result in force value for horizontally grasping direction with threshold F_2.

6. CONCLUSION

This study presented a comprehensive solution for driving manipulation using a low-cost gripper such as mechanical design, computational mechanics, and theoretical evaluation. In detail, some works have mathematically described our analysis in both forward and reverse kinematics using the FANUC robot platform. Subsequently, an appropriate control scheme based on the derived motivation was proposed. To validate our approach, several trials were conducted in both simulation and experiments within various scenarios. Based on these achievements, this work has been shown to be efficient, feasible, and applicable in real-world manufacturing systems, for example mass production, manipulation systems, and educational purposes.

For further development, the control gains should be automatically adjusted by several expert-based scheme such as fuzzy logic control, neural network control or combined scheme. On the other hand, some models of AI (Artificial Intelligence) could be considered to adapt with various objects. In the practical applications, our approach could be utilized in grasping the sensitive objects, for instance eggs, food, or soft drink. Also, it can be deployed in the supporting industries.

APPENDIX

Generally, it could be evaluated that the matrix transformation among links is established from above information in DH matrix, as following

$$ {}^{i-1}_{i}A = \begin{bmatrix} \cos\theta_i & -\sin\theta_i\cos\alpha_i & \sin\theta_i\sin\alpha_i & a_i\cos\theta_i \\ \sin\theta_i & \cos\theta_i\cos\alpha_i & -\cos\theta_i\sin\alpha_i & a_i\sin\theta_i \\ 0 & \sin\alpha_i & \cos\alpha_i & d_i \\ 0 & 0 & 0 & 1 \end{bmatrix} \quad \text{(1-A)} $$

- Relation between link 0 and link 1:

$$ {}^{0}_{1}A = \begin{bmatrix} \cos\theta_1 & 0 & \sin\theta_1 & L_1\cos\theta_1 \\ \sin\theta_1 & 0 & -\cos\theta_1 & L_1\sin\theta_1 \\ 0 & 1 & 0 & 0 \\ 0 & 0 & 0 & 1 \end{bmatrix} \quad \text{(2-A)} $$

- Relation between link 1 and link 2:

$$ {}^{1}_{2}A = \begin{bmatrix} \cos\theta_2 & -\sin\theta_2 & 0 & L_2\cos\theta_2 \\ \sin\theta_2 & \cos\theta_2 & 0 & L_2\sin\theta_2 \\ 0 & 0 & 1 & 0 \\ 0 & 0 & 0 & 1 \end{bmatrix} \quad \text{(3-A)} $$

- Relation between link 3 and link 4:

$$ {}^{3}_{4}A = \begin{bmatrix} \cos\theta_4 & 0 & \sin\theta_4 & 0 \\ \sin\theta_4 & 0 & -\cos\theta_4 & 0 \\ 0 & 1 & 0 & 0 \\ 0 & 0 & 0 & 1 \end{bmatrix} \quad \text{(4-A)} $$

Thus, the transformation matrix from end-effector to global coordinate is,

$$ {}^{0}_{5}A = \begin{bmatrix} r_{11} & r_{12} & r_{13} & p_x \\ r_{21} & r_{22} & r_{23} & p_y \\ r_{31} & r_{32} & r_{33} & p_z \\ 0 & 0 & 0 & 1 \end{bmatrix} \quad \text{(5-A)} $$

where,

$$ r_{11} = \sin\theta_1\sin\theta_5 + \cos\left(\theta_2+\theta_3+\theta_4\right)\cos\theta_1\cos\theta_5 $$

$$r_{12} = \sin\theta_1 \cos\theta_5 - \cos(\theta_2 + \theta_3 + \theta_4)\cos\theta_1 \sin\theta_5$$
$$r_{13} = \cos\theta_1 \sin(\theta_2 + \theta_3 + \theta_4)$$
$$r_{21} = \sin\theta_1 \cos\theta_5 \cos(\theta_2 + \theta_3 + \theta_4) - \cos\theta_1 \sin\theta_5$$
$$r_{22} = -\cos\theta_1 \cos\theta_5 - \sin\theta_1 \sin\theta_5 \cos(\theta_2 + \theta_3 + \theta_4)$$
$$r_{23} = \sin\theta_1 \sin(\theta_2 + \theta_3 + \theta_4)$$
$$r_{31} = \cos\theta_5 \sin(\theta_2 + \theta_3 + \theta_4)$$
$$r_{32} = -\sin\theta_5 \sin(\theta_2 + \theta_3 + \theta_4)$$
$$r_{33} = -\cos(\theta_2 + \theta_3 + \theta_4)$$

ACKNOWLEDGMENT

We acknowledge Ho Chi Minh City University of Tec–hnology, (VNU-HCM) for supporting this study.

REFERENCES

[1] Chen, X., Zhang, X., Huang, Y., Cao, L., & Liu, J. (2022). A review of soft manipulator research, applications, and opportunities. Journal of Field Robotics, 39(3), 281-311.

[2] Hentout, A., Maoudj, A., & Aouache, M. (2023). A review of the literature on fuzzy-logic approaches for collision-free path planning of manipulator robots. Artificial Intelligence Review, 56(4), 3369-3444.

[3] Tang, Y., Chen, M., Wang, C., Luo, L., Li, J., Lian, G., & Zou, X. (2020). Recognition and localization methods for vision-based fruit picking robots: A review. Frontiers in Plant Science, 11, 510.

[4] Ngo, H. Q. T. (2023). Using an HSV-based Approach for Detecting and Grasping an Object by the Industrial Manipulator System. FME Transactions, 51(4), 513.

[5] Hoai, P. L., Cong, V. D., & Hiep, T. T. (2023). Design a low-cost delta robot arm for pick and place applications based on computer vision. FME Transactions, 51(1), 99-108.

[6] Fatima, N., Massaad, E., Hadzipasic, M., Shankar, G. M., & Shin, J. H. (2021). Safety and accuracy of robot-assisted placement of pedicle screws compared to conventional free-hand technique: a systematic review and meta-analysis. The Spine Journal, 21(2), 181-192.

[7] Huang, J., Pham, D. T., Wang, Y., Ji, C., Xu, W., Liu, Q., & Zhou, Z. (2019). A strategy for human-robot collaboration in taking products apart for remanufacture. Fme Transactions, 47(4), 731-738.

[8] Samadikhoshkho, Z., Zareinia, K., & Janabi-Sharifi, F. (2019, May). A brief review on robotic grippers classifications. In 2019 IEEE Canadian Conference of Electrical and Computer Engineering (CCECE) (pp. 1-4). IEEE.

[9] Honarpardaz, M., Tarkian, M., Ölvander, J., & Feng, X. (2017). Finger design automation for industrial robot grippers: A review. Robotics and Autonomous Systems, 87, 104-119.

[10] Zhang, B., Xie, Y., Zhou, J., Wang, K., & Zhang, Z. (2020). State-of-the-art robotic grippers, gras–ping and control strategies, as well as their applications in agricultural robots: A review. Computers and Electronics in Agriculture, 177, 105694.

[11] Antonelli, D., & Bruno, G. (2019). Dynamic distribution of assembly tasks in a collaborative workcell of humans and robots. FME Transactions, 47(4), 723-730.

[12] Lu, Y., Xie, Z., Wang, J., Yue, H., Wu, M., & Liu, Y. (2019). A novel design of a parallel gripper actuated by a large-stroke shape memory alloy actuator. International Journal of Mechanical Sciences, 159, 74-80.

[13] Zhang, P., & Tang, B. (2022). A two-finger soft gripper based on bistable mechanism. IEEE Robotics and Automation Letters, 7(4), 11330-11337.

[14] Cong, V. D. (2021). Industrial robot arm controller based on programmable system-on-chip device. FME Transactions, 49(4), 1025-1034.

[15] Cortez, W. S., Oetomo, D., Manzie, C., & Choong, P. (2019). Control barrier functions for mechanical systems: Theory and application to robotic grasping. IEEE Transactions on Control Systems Technology, 29(2), 530-545.

[16] Ficuciello, F., Migliozzi, A., Laudante, G., Falco, P., & Siciliano, B. (2019). Vision-based grasp learning of an anthropomorphic hand-arm system in a synergy-based control framework. Science robotics, 4(26), eaao4900.

[17] Zaidi, S., Maselli, M., Laschi, C., & Cianchetti, M. (2021). Actuation technologies for soft robot grippers and manipulators: A review. Current Robotics Reports, 2(3), 355-369.

[18] Gorjup, G., Gao, G., Dwivedi, A., & Liarokapis, M. (2020). Combining compliance control, cad based localization, and a multi-modal gripper for rapid and robust programming of assembly tasks. In 2020 IEEE/RSJ International Conference on Intelligent Robots and Systems (IROS) (pp. 9064-9071). IEEE.

[19] Xu, W., Zhang, H., Yuan, H., & Liang, B. (2021). A compliant adaptive gripper and its intrinsic force sensing method. IEEE Transactions on Robo–tics, 37(5), 1584-1603.

[20] Zhang, T., Huang, Z., You, W., Lin, J., Tang, X., & Huang, H. (2019). An autonomous fruit and vegetable harvester with a low-cost gripper using a 3D sensor. Sensors, 20(1), 93.

[21] Hoang, T. T. et al. (2021). Soft robotic fabric gripper with gecko adhesion and variable stiffness. Sensors and Actuators A: Physical, 323, 112673.

[22] Ngo, T. H. et al. (2018). Design and kinetostatic modeling of a compliant gripper for grasp and autonomous release of objects. Advanced Robo–tic, 32(14), 717-735.

[23] Vo, Q. N., Huynh, T. T., Dao, S. V. (2022). App–lying Soft Actuator Technology for Hand Rehabi–litation. In 8th International Conference on the Development of Biomedical Engineering in Viet–

nam: Proceedings of BME 8, 2020, Vietnam: Healthcare Technology for Smart City in Low-and Middle-Income Countries (pp. 123-132). Springer International Publishing.

[24] Quach, B. M., Van Toi, V., Pham, H. T. T. (2022). Design of a soft robotic glove for hand rehabilitation based on pneumatic network method and low cost electro-pneumatic device. In 8th Inter–national Conference on the Development of Bio–medical Engineering in Vietnam: Proceedings of BME 8, 2020, Vietnam: Healthcare Technology for Smart City in Low-and Middle-Income Countries (pp. 101-111). Springer International Publishing.

[25] Anh-My, C. (2021). Effective Solution to Integrate and Control a Heavy Robot Driven by Hydraulic Actuators. Further Advances in Internet of Things in Biomedical and Cyber Physical Systems, 331-345.

[26] Do, T. T., Nguyen, Q. H., & Chu, D. H. (2022). An open-architecture integration solution for the rese–arch and development of smart robots. Vietnam Journal of Science, Technology and Engineering, 64(4), 36-44.

[27] Nguyen, T. H., Nguyen, T. T., Tran, T. V. (2021). A method for localizing and grasping objects in a picking robot system using kinect camera. In Intelligent Human Computer Interaction: 12th International Conference, IHCI 2020, Daegu, South Korea, November 24–26, 2020, Proceedings, Part II 12 (pp. 21-26). Springer International Publishing.

[28] Hoang, H. H., Tran, B. L. (2021). Accurate ins–tance-based segmentation for boundary detection in robot grasping application. Applied Sciences, 11(9), 4248.

[29] Le, T. T., Le, T. S., Chen, Y. R., Vidal, J., & Lin, C. Y. (2021). 6D pose estimation with combined deep learning and 3D vision techniques for a fast and accurate object grasping. Robotics and Auto–nomous Systems, 141, 103775.

[30] Hoang, D. C., Stork, J. A., Stoyanov, T. (2022, May). Context-Aware Grasp Generation in Clut–tered Scenes. In 2022 International Conference on Robotics and Automation (ICRA) (pp. 1492-1498). IEEE.

[31] Pham, H. D., Okata, Y., Vu, H. M., Tran, N. X., Nguyen, Q. T., & Nguyen, L. T. (2019). Robotic-assisted surgery for choledochal cyst in children: early experience at Vietnam National Children's Hospital. Pediatric Surgery International, 35, 1211-1216.

[32] Lam, C. T., Phung, T. C. (2021). Research on app–lication of industrial robots in automated fueling systems for small individual cars. VNUHCM Jour–nal of Engineering and Technology, 4(3), 1057-1067.

[33] Ji, W., Zhang, J., Xu, B., Tang, C., Zhao, D. (2021). Grasping mode analysis and adaptive impedance control for apple harvesting robotic grippers. Com–puters and Electronics in Agriculture, 186, 106210.

[34] Ji, W., Tang, C., Xu, B., He, G. (2022). Contact force modeling and variable damping impedance control of apple harvesting robot. Computers and Electronics in Agriculture, 198, 107026.

[35] Liang, H., Ma, X., Li, S., Görner, M., Tang, S., Fang, B., ... Zhang, J. (2019, May). Pointnetgpd: Detecting grasp configurations from point sets. In 2019 International Conference on Robotics and Automation (ICRA) (pp. 3629-3635). IEEE.

[36] Turco, E., Bo, V., Pozzi, M., Rizzo, A., Prattichizzo, D. (2021). Grasp planning with a soft reconfigurable gripper exploiting embedded and environmental constraints. IEEE Robotics and Automation Letters, 6(3), 5215-5222.

[37] Wan, F., Wang, H., Wu, J., Liu, Y., Ge, S., & Song, C. (2020). A reconfigurable design for omni-adap–tive grasp learning. IEEE Robotics and Automation Letters, 5(3), 4210-4217.

[38] Xu, S., He, B., Zhou, Y., Wang, Z., & Zhang, C. (2019). A hybrid position/force control method for a continuum robot with robotic and environmental compliance. IEEE Access, 7, 100467-100479.

[39] Hernandez-Mendez, S., Marin-Hernandez, A., Palacios-Hernandez, E. R., & Luna-Gallegos, K. L. (2017). A switching position/force controller for two independent finger gripper over ROS. In 2017 International Conference on Electronics, Communi-cations and Computers (CONIELECOMP) (pp. 1-6). IEEE.

NOMENCLATURE

a_i	distance from Z_i axis to Z_{i+1} axis
α_i	angular rotation from Z_i axis to Z_{i+1} axis from the view of X_{i+1} axis
d_i	distance from X_i axis to X_{i+1} axis
θ_i	angular rotation from X_i axis to X_{i+1} axis from the view of Z_i axis
d_1,d_2	distance between two base points AB and CD
d_3,d_4	distance between two base points AD and BC
L_1,L_2,L_3	length of links
α	angle between two base points

ИСТРАЖИВАЊЕ МЕХАНИЧКОГ ДИЗАЈНА РОБОТСКЕ ХВАТАЉКЕ ЗА ИНТЕЛИГЕНТНО УПРАВЉАЊЕ ПОМОЋУ ЈЕФТИНОГ СЕНЗОРА

Т.Т. Нгујен, Т.Х. Нгујен, Х.К.Т. Нго

Са појавом индустрије 4.0, постоји растућа потреба за интелигентним и аутоматизованим роботским системима способним да обављају сложене задатке у непознатим окружењима. Овај рад се фокусира на развој механичког дизајна за роботску хватаљку и имплементацију интелигентне манипулације за бирање мете помоћу ФАНУЦ роботске платформе. Предложени метод комбинује рачунарску механику за хватач, напредне технике контроле покрета и стратегију контроле хватања како би се омогућила руци робота да прецизно и ефикасно идентификује и

одабере циљни објекат. Да бисмо потврдили наш приступ, спроведено је неколико експерименталних валидација у различитим сценаријима. Добро је познато да је предложени рад изводљив, ефикасан и применљив за широк спектар индустријских примена.